



ELSEVIER

Physica D 168–169 (2002) 93–105

PHYSICA D

www.elsevier.com/locate/physd

# Using advection to control the velocity of patterns in rings of maps

Pedro G. Lind<sup>a,b,c</sup>, João A.M. Corte-Real<sup>a,c</sup>, Jason A.C. Gallas<sup>a,b,c,d,\*</sup>

<sup>a</sup> *Unidade de Meteorologia e Climatologia, Instituto de Ciência Aplicada e Tecnologia, Faculdade de Ciências, Universidade de Lisboa, 1749-016 Lisboa, Portugal*

<sup>b</sup> *Instituto de Física, Universidade Federal do Rio Grande do Sul, 91501-970 Porto Alegre, Brazil*

<sup>c</sup> *Centro de Geofísica, Universidade de Évora, 7000 Évora, Portugal*

<sup>d</sup> *Institut für Computer Anwendungen, Universität Stuttgart, Pfaffenwaldring 27, D-70569 Stuttgart, Germany*

## Abstract

Traveling patterns are well-known features of rings of symmetrically coupled maps which, however, propagate with rather small velocities, of the order of  $\sim 10^{-3}$  sites per step. We show that it is easy to produce traveling patterns with velocities tunable over three orders of magnitude by simply breaking the symmetry of the coupling between neighbors. This asymmetry arises naturally when the usual model of coupled map lattices is generalized to also include advection. In addition, asymmetries change the wavelength of waves traveling on the lattice.

© 2002 Elsevier Science B.V. All rights reserved.

PACS: 05.45.Ra; 47.25.Ac

Keywords: Spatio-temporal Chaos; Coupled map lattices; Asymmetric coupling; Velocity control

## 1. Introduction

The forecasting of atmospheric systems from a given set of measurements of physical quantities (e.g. pressure, temperature, etc.) in space and time is well known to be a quite hard task [1–5]. Weather forecasts are usually obtained either by numerical integration of the differential equations controlling the atmospheric system [3] or by nonlinear analysis of observed time-series [6]. To reduce the time of computation and to investigate the dynamics over longer time intervals, it is a common practice to neglect certain terms in such equations, maintaining only those judged dominant [1–3].

One such approximation concerns atmospheric systems away from the boundary layer (ground), where friction is neglected, and leads to a set of differential equations known as *gradient flows* [4]. Gradient flows can explain the existence of circulating systems in the atmosphere such as highs and lows [5]. On the other hand, one of the most prominent terms in the governing equations, present in virtually all approximations, is that involving advection by the horizontal wind [2,5].

In this paper, we show that an interesting new class of models for atmospheric simulations, containing a term representing directly advection in a system, may be obtained by slightly extending the generic class of discrete models known as *coupled map lattices*, popular nowadays to investigate spatio-temporal complexity [7,8]. Results obtained with this new model reproduce qualitatively several aspects of the

\* Corresponding author. Present address: Instituto de Física, Universidade Federal do Rio Grande do Sul, 91501-970 Porto Alegre, Brazil. Fax: +55-51-3316-7286.

E-mail address: jgallas@if.ufrgs.br (J.A.C. Gallas).

phenomenology observed in the presence of gradient flows. This model allows a number of interesting investigations and the purpose of this paper is to report part of what we have obtained so far.

The majority of applications of lattices of coupled maps, either numerical [8] or analytical [9,10], consider the dynamics controlled by the equation

$$x_{t+1}(i) = f(x_t(i)) + \varepsilon D_{i,t}, \quad (1)$$

where  $t = 0, 1, \dots$  represents a discrete time variable,  $i$  the discrete sites composing the lattice,  $f(x)$  the ‘force’ acting locally and  $D_{i,t}$  a discretization of the Laplacian operator responsible for the diffusion along the lattice. When subjected to periodic boundary conditions,  $x_1 \equiv x_{L+1}$ ,  $L$  being the total number of sites, the one-dimensional lattice of Eq. (1) is, effectively, a *ring* of coupled maps (RCMs). This very popular ring model will be extended here to incorporate advection.

As known [8], when initializing each site  $i$  with arbitrary initial conditions and letting the lattice ‘thermalize’ for a suitable transient time, the system is seen to approach an asymptotic state, a ‘pattern’, which is a member of a large family of possible states (attractors). Subsequently to the transient, the patterns display time-evolutions with or without space and/or time periodicities. The classification of possible time-evolutions for patterns is an interesting subject, particularly the phenomena connected with the appearance of *traveling waves* on the lattice [8,11–15]. However, a remarkable characteristic observed in all results based on the purely diffusive model of Eq. (1) is that the velocity of patterns moving in the ring is invariably small, of the order of  $\simeq 10^{-3}$  sites per step, at most.

The purpose of this paper is to introduce a simple generalization of the diffusive model in Eq. (1), a new model given by

$$x_{t+1} = f(x_t(i)) + \varepsilon D_{i,t} - \gamma A_{i,t}, \quad (2)$$

where  $A_{i,t}$ , defined below in Eq. (5), represents the advection in the lattice, with its amplitude controlled by the parameter  $\gamma$ . As shown in the next section, the introduction of advection is quite a natural step when considering the physics of complex phenomena (e.g. convection is a crucial mechanism in the dynamics of

large-scale atmospheric motions) and yields a more realistic model which contains Eq. (1) as a particular case. An important advantage of considering advection is that this new contribution provides a rather effective means of tuning and controlling the velocity of traveling waves and patterns on the lattice. The ability of tuning velocities is an interesting feature for a number of applications in geophysics.

A number of previous works has already considered using asymmetrically coupled maps to simulate flow systems [16–20] and in the context of renormalization group analysis [10]. However, as shown in the next section, instead of postulating asymmetries in a somewhat ad hoc manner, here we start from a discretization of the relevant differential operators and use periodic boundary conditions to simulate systems in which effects of circulation are important, as is the case of the atmosphere. This approach provides a clear and simple physical interpretation for the asymmetry.

The derivation and the physical meaning of the advection term  $A_{i,t}$  are presented in Section 2. Numerical results for rings of coupled maps with advection and the analogy with gradient flows are discussed in Section 3. A number of interesting results concerning the spatial periodicity are shown in Section 4. Finally, our conclusions are in Section 5.

## 2. A simple model of advection

The two fundamental quantities underlying the model are (i) the diffusion  $\nabla^2 f$ , and (ii) the advection  $\bar{v} \cdot \bar{\nabla} f$ . Discretizing them, as usual [3], one finds

$$v \frac{df}{dx} \sim v \frac{f(x + \Delta x) - f(x - \Delta x)}{2\Delta x}, \quad (3)$$

$$\frac{d^2 f}{dx^2} \sim \frac{f(x + \Delta x) - 2f(x) + f(x - \Delta x)}{(\Delta x)^2}. \quad (4)$$

For unitary increments and with the abbreviations

$$A_{i,t} = \frac{f(x_t(i+1)) - f(x_t(i-1))}{2}, \quad (5)$$

$$D_{i,t} = \frac{f(x_t(i+1)) + f(x_t(i-1))}{2} - f(x_t(i)), \quad (6)$$

the above equations simplify to

$$v \frac{df}{dx} \sim vA_{i,t}, \quad (7)$$

$$\frac{d^2 f}{dx^2} \sim 2D_{i,t}. \quad (8)$$

Now, we start from the standard equation ruling the dynamics of coupled maps [8] and slightly extend it by introducing to it a new parameter  $\gamma$  as follows:

$$x_{t+1}(i) = (1 - \varepsilon)f(x_t(i)) + \frac{\varepsilon + \gamma}{2}f(x_t(i - 1)) + \frac{\varepsilon - \gamma}{2}f(x_t(i + 1)). \quad (9)$$

By rearranging terms, this equation may be easily brought to the simple form of Eq. (2) where, in addition to the familiar diffusive term  $D_{i,t}$  controlled by  $\varepsilon$ , the new degree of freedom controlled by  $\gamma$  corresponds to the advection  $A_{i,t}$ . Eqs. (2) and (7) strongly suggest that  $\gamma$  has the physical meaning of a circulation velocity. As discussed below, this is indeed the case.

The coupling strength  $\varepsilon$  varies between 0 (un-coupled regime) and 1 (totally coupled regime). The valid range of  $\gamma$  depends on  $\varepsilon$  and, observing that  $(\varepsilon \pm \gamma)/2$  should also lie in  $[0, 1]$ , it is readily found to be  $-\varepsilon \leq \gamma \leq \varepsilon$ .

For  $\gamma = 0$  one recovers the usual diffusive model while both extrema,  $\gamma = \varepsilon$  and  $-\varepsilon$ , correspond to the situations referred to as ‘one-way coupling’ [16,17,21], one for each direction of motion in the ring.

### 3. The effect of advection

We now study the effect of advection for a RCMs ruled by the usual *logistic* local interactions, namely, by

$$f(x) = 1 - ax^2. \quad (10)$$

In the absence of asymmetries (i.e. for  $\gamma = 0$ ), the dynamics of this paradigmatic ring was considered in detail recently [22], where it has been shown that the parameter region delimited by  $1.6 \leq a \leq 1.85$ , with

coupling strength  $\varepsilon \geq 0.4$ , is the most interesting for investigating the dynamics of traveling waves.

Generic characteristics of traveling waves in this region are [8,22]:

- (1) Velocity distributions which are symmetric and ‘quantized’ as functions of  $a$ .
- (2) The magnitude of the velocity increase linearly with  $a$ .
- (3) The slope of the linear dependence on  $a$  is modulated by the coupling strength  $\varepsilon$ .
- (4) The velocity of traveling waves is invariably small, of the order of  $10^{-3}$  sites per step.

We now investigate what happens with these characteristics in systems where advection is present, i.e. when  $\gamma \neq 0$  in Eq. (2).

#### 3.1. Velocity dependence on asymmetric coupling

Fig. 1 shows velocity distributions as a function of  $a$  for a few representative values of  $\gamma$ . The interval  $1.6 < a < 1.85$  was divided into 100 parts and for each value of  $a$  we plot 100 velocities, obtained from a different set of random initial conditions. For reference, a typical distribution for symmetric coupling ( $\gamma = 0$ ) is also shown in Fig. 1(a). The mechanism of velocity selection in bands (‘quantization’) is explained [7] as the number of phase slips in the lattice.

As is clear from the figures, by increasing the asymmetry it is now possible to obtain much higher velocities, up to 100 times higher than those obtained with symmetric coupling. Increasing  $\varepsilon$  to 1, the interval of  $\gamma$  gets wider ( $-\varepsilon \leq \gamma \leq \varepsilon$ ) and, consequently, the velocity may be tuned up to 1000 times higher, whenever  $\gamma \sim \pm\varepsilon$ . In addition, the distributions of positive and negative velocities are symmetric with respect to the line  $v = \gamma$ , thus suggesting a mechanism for ‘directional segregation’: velocities for positive (negative) values of  $\gamma$  tend to be positive (negative). Such directional segregation mechanism is rather *different* from that responsible for the velocity selection in bands.

Velocity values spread around a small interval around  $v = \gamma$  and remain ‘quantized’ for  $\gamma \neq 0$ . Nevertheless, the global shape of the velocity distributions changes, spreading around  $v = \gamma$  but asymmetrically.

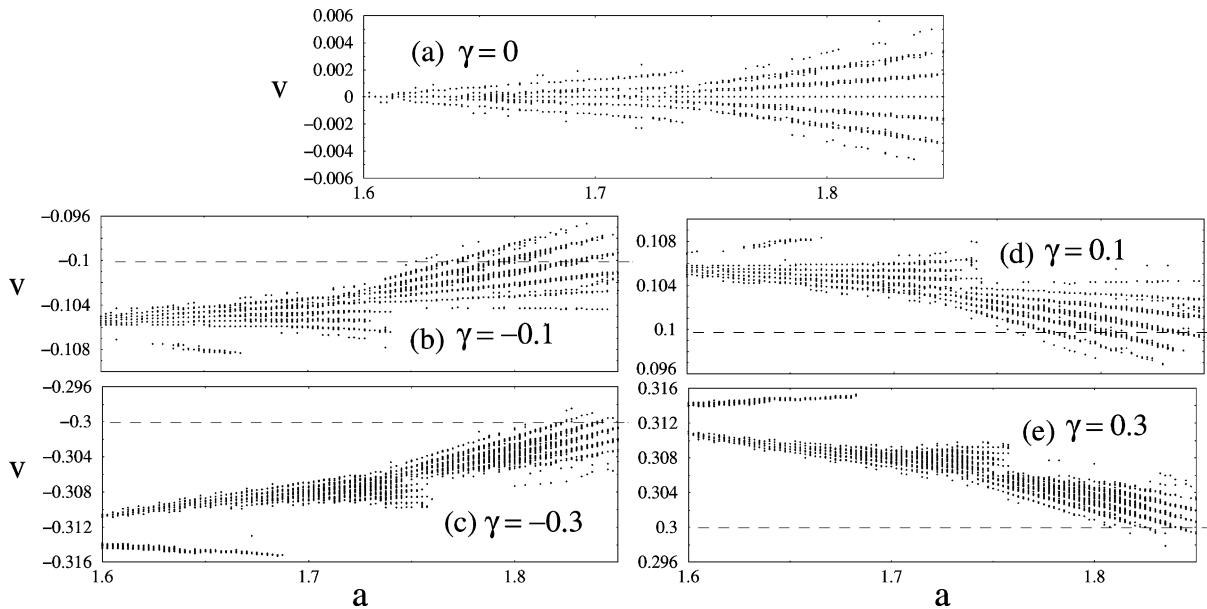


Fig. 1. Typical velocity distributions as a function of the local nonlinearity  $a$ , for representative values of  $\gamma$ , on a ring with  $L = 64$ ,  $\varepsilon = 0.5$ . Dashed lines indicate  $v = \gamma$ . Notice the differences in the vertical scales.

An exception is observed for the one-way coupling,  $\gamma = \pm\varepsilon$ , where velocity distributions collapse leading always to the same value,  $v = \gamma$ .

The increase in the velocity due to the asymmetry is greater than the velocity spread due to diffusion so that in this regime *advection dominates diffusion*. This behavior is similar to what happens for atmospheric air masses with a certain temperature surrounded by an environment at a different temperature. The existence of two temperatures implies the diffusion of heat (Laplacian equation), either if the air mass moves or not. In the presence of wind, the air mass moves, adding an advection term in the thermodynamic equation [5,23]. Usually, observational data show that air masses tend to maintain their temperatures, which means that advection is predominant over diffusion.

An interesting additional feature in Fig. 1 is the abrupt ‘cut’ observed in the velocity distributions for  $a \sim 1.73$ . As known, this value marks the beginning of the period-3 window of the local map. The relation between period-3 windows and the changes of distributions remains unclear to us.

### 3.2. Controlling the velocity of traveling waves

As seen in the previous section, velocities are mainly dominated by advection. In this section, we argue that the velocities are not only dominated by advection but, in fact, that the velocity  $v$  is actually given by the parameter  $\gamma$ , i.e.  $v = \gamma$ .

Fig. 2 shows the velocity as a function of  $\gamma$  for two representative values of  $a$ , as observed on a lattice with  $L = 64$  and  $\varepsilon = 0.5$ . In both examples, the top figures show the asymptotic pattern on the lattice, as obtained after a transient of 50,000 time-steps, always from the same random initial condition. In both cases, the next three figures display under successive magnifications that the velocity (i) varies linearly with  $\gamma$ , a fact that is easily corroborated by a fit to the data, and (ii) may contain a ‘microscopic substructure’.

As is clear from the figure, the microscopic variation depends whether or not the local parameter  $a$  lies below the accumulation point  $a_\infty \simeq 1.401155\dots$  characteristic of the  $2^n$  cascade [24]. For  $a < a_\infty$ , the microscopic substructure is given by a stair-shaped function that remains essentially constant within a

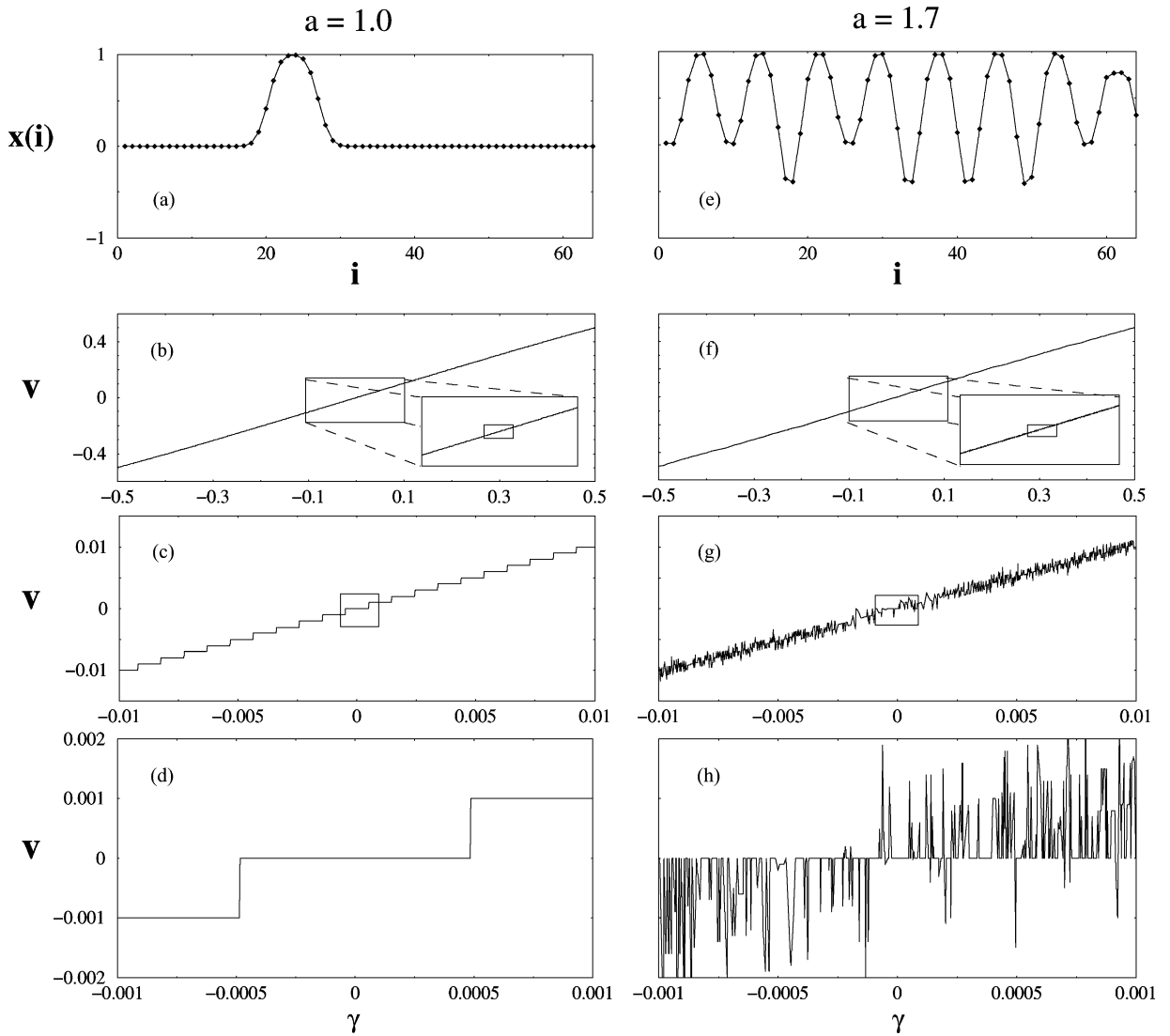


Fig. 2. Velocity dependence with  $\gamma$  for two representative values of  $a$ , for a lattice with  $L = 64$  and  $\varepsilon = 0.5$ . As the zooms show, there are two different types of microscopic substructuring (see text).

given interval, with very sharp transitions. On the other hand, for  $a > a_\infty$ , the microscopic substructure presents random fluctuations around  $v = \gamma$ . The interval of these fluctuations is of the same order as the spread in  $v$  shown in Fig. 1.

Similar results are obtained for other values of  $L$  as is illustrated in Fig. 3.

All results so far were obtained for  $\varepsilon = 0.5$ , which is representative of what one sees for  $\varepsilon \geq 0.4$ . As shown

by Fig. 4, the velocity dependence with  $\gamma$  is no longer linear, in the weak coupling regime  $\varepsilon < 0.4$  and below the accumulation point. In particular, notice the existence of a locking interval  $[-\gamma_\ell, \gamma_\ell]$  centered around  $\gamma = 0$ . Outside the locking interval, we find  $v \propto |\gamma|^\alpha$  with  $0 < \alpha \leq 1$ . In the weak coupling regime,  $\alpha$  grows with  $\varepsilon$ , reaching the value  $\alpha = 1$  for  $\varepsilon \simeq 0.2$ .

Therefore, for  $a < a_\infty$ , the weak coupling regime is characterized by a velocity given approximately by

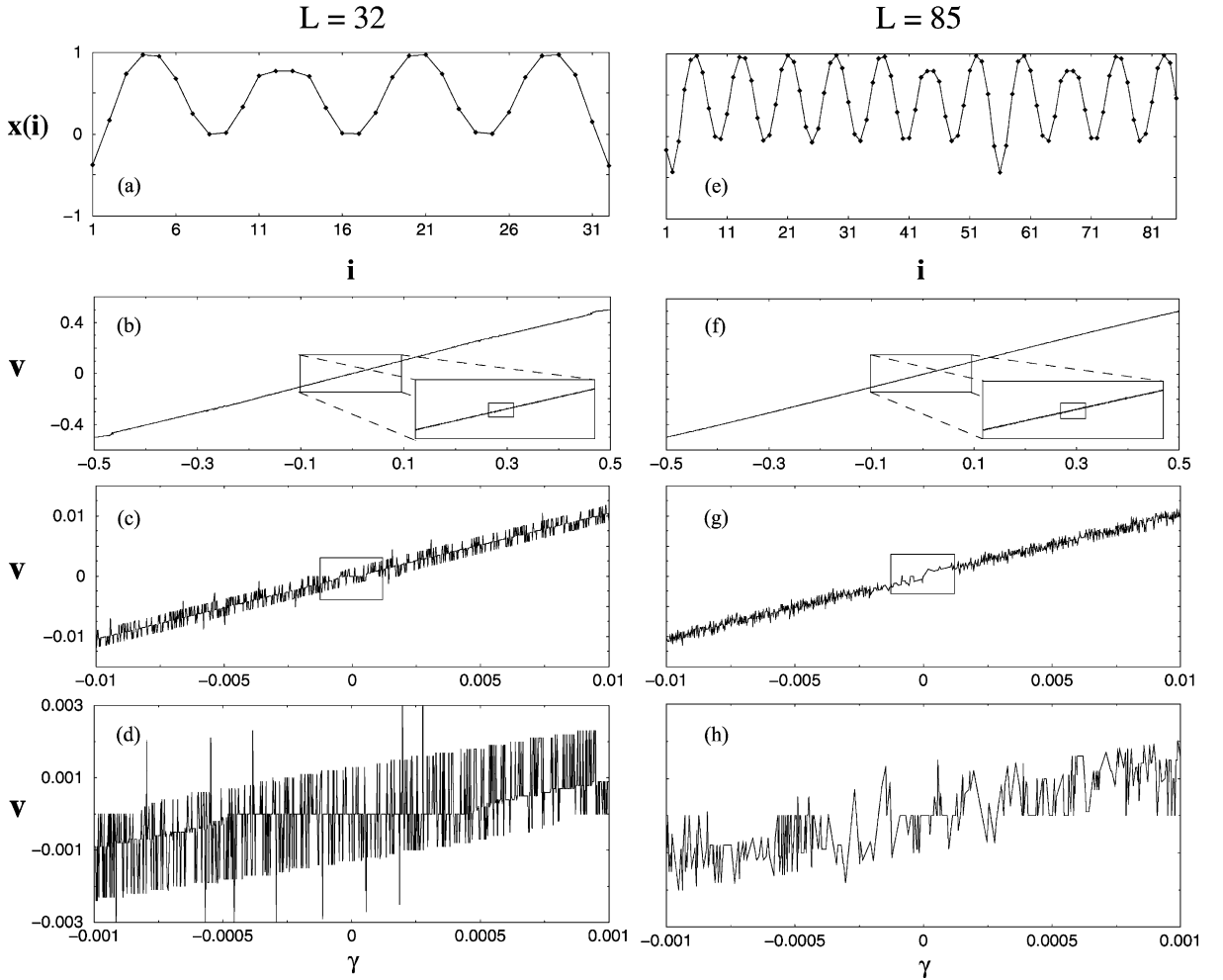


Fig. 3. The shape and velocity of patterns do not depend significantly on the lattice size  $L$ . Notice that both patterns on the lattice, (a) and (e), are roughly sinusoidal with a wavelength of eight sites. Here  $a = 1.7$  and  $\varepsilon = 0.5$ .

$v = 0$  when  $|\gamma| \leq \gamma_\ell$  and by

$$v = \frac{\gamma}{|\gamma|} (|\gamma| - \gamma_\ell)^\alpha + \theta \quad (11)$$

when  $\gamma_\ell \leq |\gamma| \leq \varepsilon$ , where  $\theta$  is the fluctuation due to the step-function substructure. The step-function substructure may still be seen, but having smaller steps. Above  $\varepsilon \sim 0.2$ , the velocity depends always linearly with  $\gamma$  ( $\alpha = 1$ ).

For  $a > a_\infty$ , there are essentially no periodic time-evolutions in the weak coupling [25].

### 3.3. Velocity in atmospheric gradient flows

The purpose of this section is to show that, essentially,  $\gamma$  is a wind velocity component, namely the *geostrophic wind* [4]

$$v_g = -\frac{1}{f\rho} \frac{\partial p}{\partial n}, \quad (12)$$

where  $p$  is the pressure,  $f \sim 10^{-4} \text{ s}^{-1}$  the mid-latitudes Coriolis parameter,  $\rho$  the density and  $\vec{n}$  the transverse natural coordinate, directed to the left of the motion and perpendicular to it.

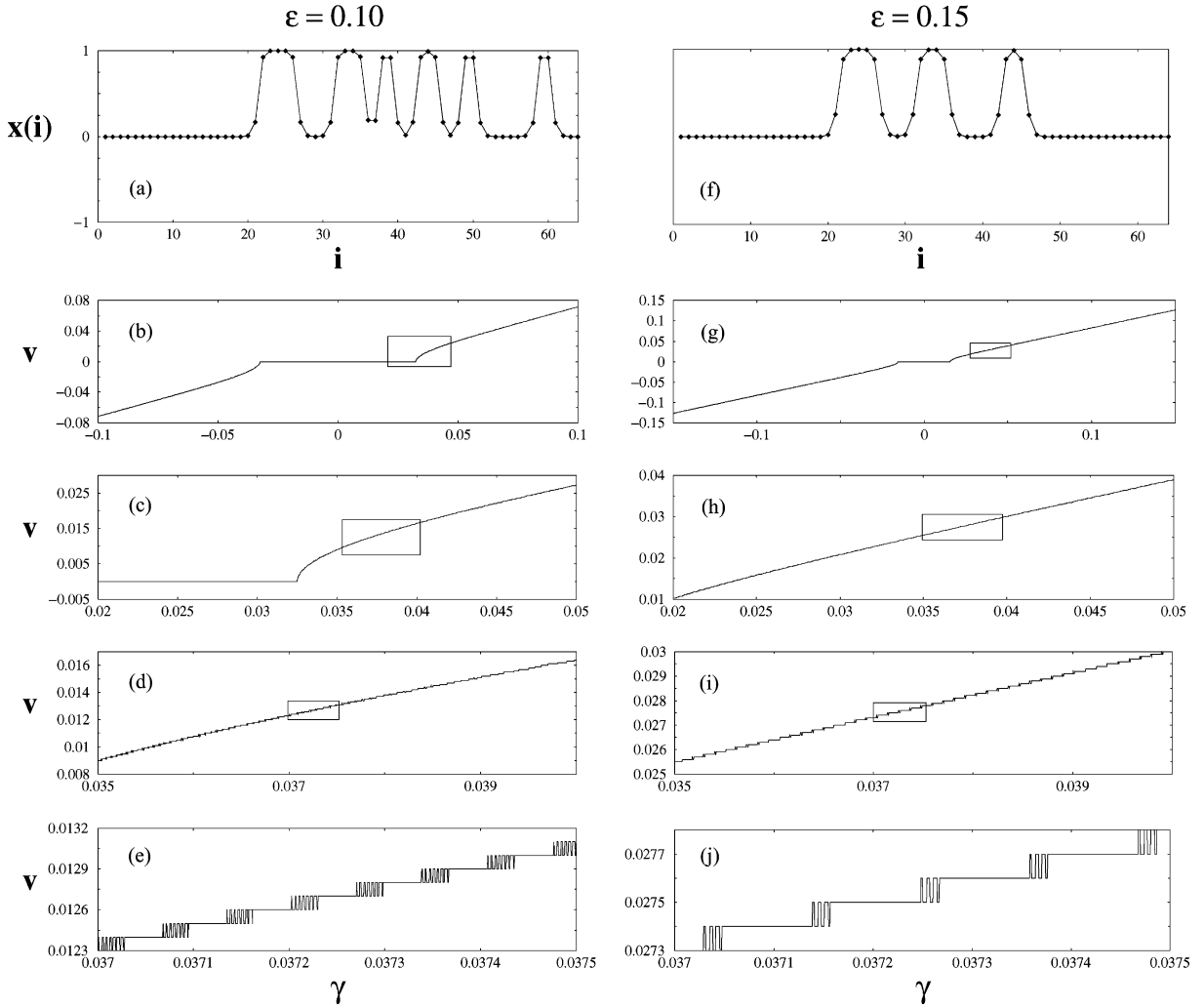


Fig. 4. Nonlinear dependence of the velocity as a function of  $\gamma$  for two typical values of  $\varepsilon$  in the weak coupling regime. A clear locking of the velocity is seen for a symmetrical interval about  $\gamma = 0$ . The boundary of that interval is given by  $\gamma_\ell \sim 0.03$ . Outside this locking interval, the velocity is proportional to  $\gamma^\alpha$ , with  $0 < \alpha \leq 1$ . For  $\varepsilon = 0.1$  and  $0.15$ , we find  $\alpha = 0.7$  and  $0.75$ , respectively. Here  $a = 1$  and  $L = 64$ .

Atmospheric highs and lows are typical examples of gradient flow systems composed by air masses with certain temperature distributions, which rotate in closed trajectories [4]. Away from the ground (boundary layer), friction forces may be neglected yielding a wind velocity given by [5]

$$v = \pm \left( \frac{f^2 R^2}{4} + f R v_g \right)^{1/2} - \frac{f R}{2} \quad (13)$$

where  $R$  is the curvature radius of the trajectory and  $R$ ,  $f$  and  $\rho$  are considered to be constants. Eq. (13)

is the velocity of the real wind, also called gradient wind since the system satisfies gradient flow conditions [4]. On the other hand, the geostrophic wind is the non-accelerating wind component.

As it is easy to see, Eqs. (11) and (13) have the same functional dependence. In particular, the optimal value  $\alpha = 0.5$  is obtained for  $\varepsilon \sim 0.06$ , in the weak coupling regime. In this case, one recognizes that the asymmetry  $\gamma$  plays the role of the geostrophic wind  $v_g$ . Furthermore, by comparing  $|\gamma|/\gamma_\ell$  with  $(fR)/(4v_g)$  for the typical (mesoscale) values  $R \sim 10^5$  m and

$v_g \sim 10$  m/s, we find  $(fR)/(4v_g) \sim 0.25$  and, from Fig. 4,  $\gamma_\ell/|\gamma| \sim 0.3$ , in quite good agreement.

#### 4. Spatial periodicity of wave-like patterns modulated by asymmetry

In the previous section, we presented results showing that it is possible to use advection to control the velocity of traveling waves in rings of maps. Another interesting feature due to advection is the possibility of modulating the spatial periodicity which underlies wave-like patterns.

Fig. 5 (left column) shows typical wave-like patterns abundant in the region delimited by  $1.6 \leq a \leq 1.85$  and  $\varepsilon \geq 0.4$ . Although such patterns are not perfectly sinusoidal, the figure shows that it is possible to associate a wavelength  $\lambda$  to each of them. This wavelength remains constant in time.

Instead of attempting to measure wavelengths directly from the asymptotic pattern on the lattice, it is

better to use a smoother function of the pattern. To this purpose, we use the spatial correlation function

$$C(i, j) = \frac{\langle x_i x_j \rangle - \langle x_i \rangle \langle x_j \rangle}{\langle x_i^2 \rangle - \langle x_i \rangle^2}, \quad (14)$$

where  $i$  and  $j$  label the space and  $\langle X \rangle$  represents a time average of  $X$  over  $\sim 10^4$  time-steps, computed after a transient of  $10^5$  time-steps. For each pattern, one has  $L$  ‘different’  $C(i, j)$  as functions of  $i$ . For each of them, the wavelength is given by  $\lambda = L/p$ , where  $p$  counts the number of local maxima. The final wavelength is given by the average of these  $L$  auxiliary wavelengths. The spatial correlations are independent of the reference site used to compute their wavelengths.

Fig. 5 clearly shows that the wavelength depends of the asymmetry  $\gamma$ , while Fig. 6 displays such dependence via wavelength histograms computed from a set of 50 random initial conditions determined for the full range of  $\gamma$ . As seen in this figure, for a fixed value of  $\gamma$ , the wavelength remains essentially constant, namely, it is independent of the initial condition

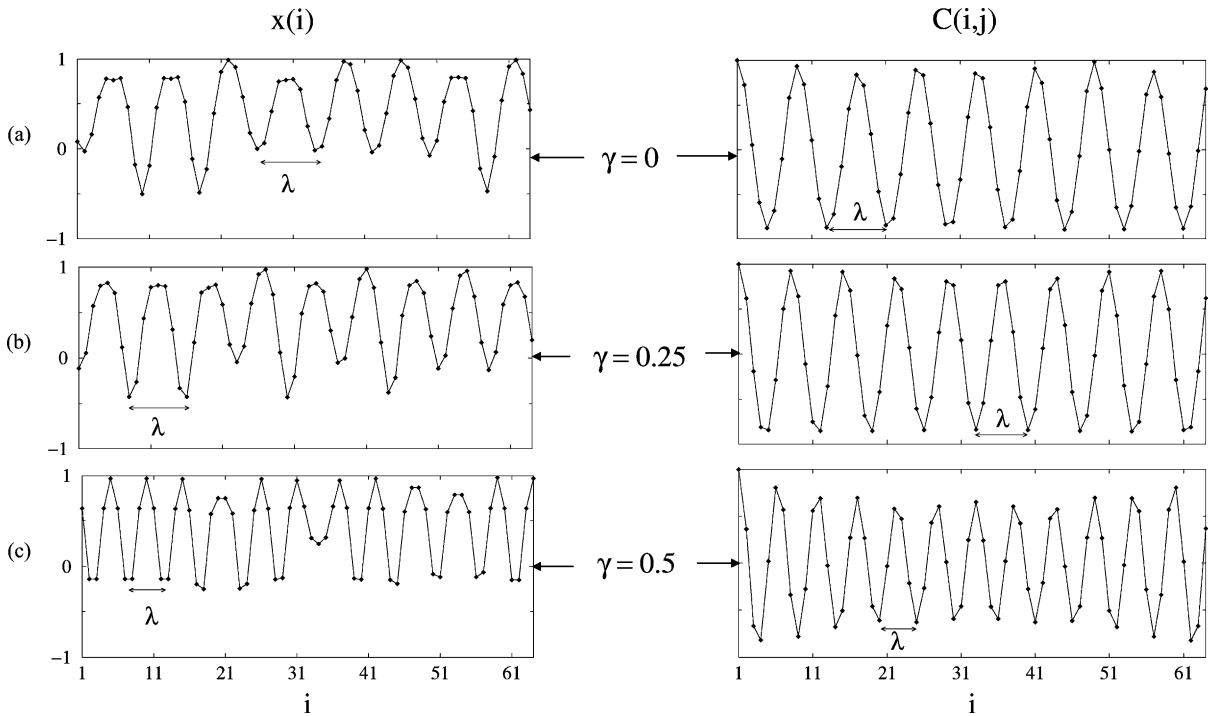


Fig. 5. The wavelength of the asymptotic patterns (left column) is the same as that of the corresponding spatial correlation  $C(i, j)$  (right column). Parameter values are  $a = 1.7$ ,  $\varepsilon = 0.5$  and  $L = 64$  for (a)  $\gamma = 0$ , (b)  $\gamma = \varepsilon/2$ , (c)  $\gamma = \varepsilon$ .

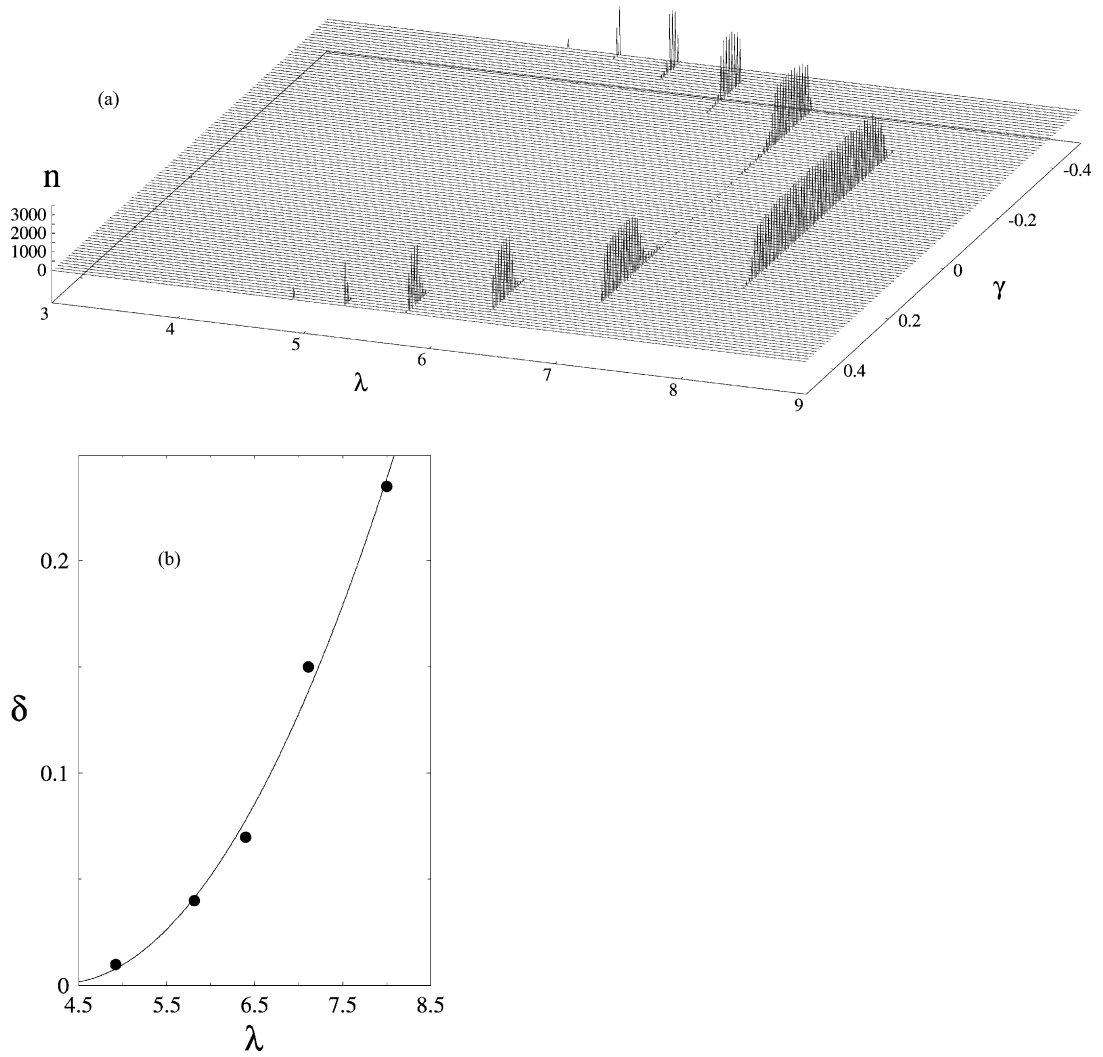


Fig. 6. Dependence of the wavelength on the parameter of asymmetry: (a) histograms displaying sudden changes of the wavelength; (b) the width  $\delta$  of the intervals where  $\lambda$  remains constant is approximately proportional to  $\lambda^2$ , the continuous curve. Here  $L = 64$ ,  $a = 1.7$  and  $\varepsilon = 0.5$ .

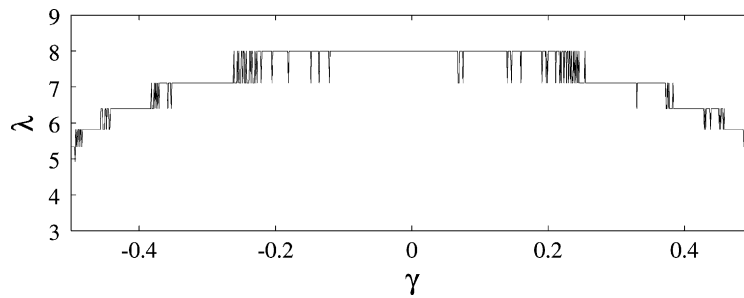
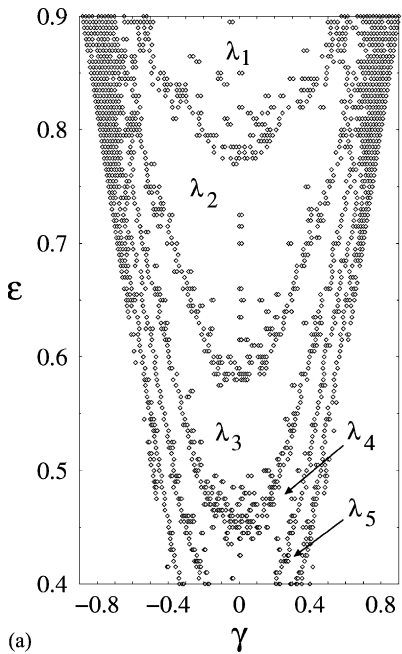


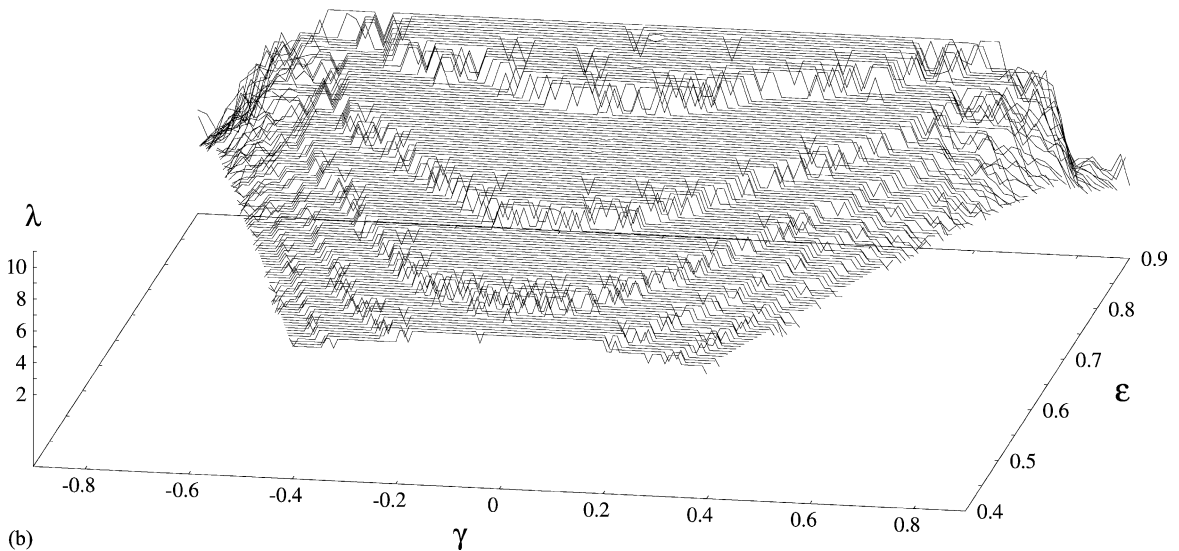
Fig. 7. The transition between plateaus displays 'hesitation' between two wavelengths. The plot shows wavelengths computed for 1000 values of  $\gamma$ , from a fixed random initial condition. Different initial conditions give similar results. Here  $L = 64$ ,  $a = 1.7$  and  $\varepsilon = 0.5$ .

imposed. Symmetric values of the asymmetry parameter have the same wavelength. The wavelength reaches its maximum of  $\lambda \sim 8$  site for a certain interval around  $\gamma_0 = 0$ . Outside this interval, there are characteristic values  $\gamma_k$ ,  $k = \pm 1, \pm 2, \dots$ , of the parameter of asymmetry where the wavelength

abruptly changes, corresponding to the appearance of an extra oscillation in the pattern. For a fixed sequence of indices, e.g. positive, the wavelength is constant inside the interval  $[\gamma_{k-1}, \gamma_k]$ , which we call “plateau”. The characteristic values  $\gamma_k$  vary linearly with  $\lambda$ .



(a)



(b)

Fig. 8. The plateaus of constant  $\lambda$ . The tri-dimensional view (on the right) is shown projected in the  $\gamma \times \varepsilon$  plane (on the left), displaying the transitions  $\lambda_k$ . In the wave-like pattern region, other values of  $L$  show similar results. Here  $L = 64$ ,  $a = 1.7$  for  $100 \times 100$  values of  $\gamma \times \varepsilon$ .

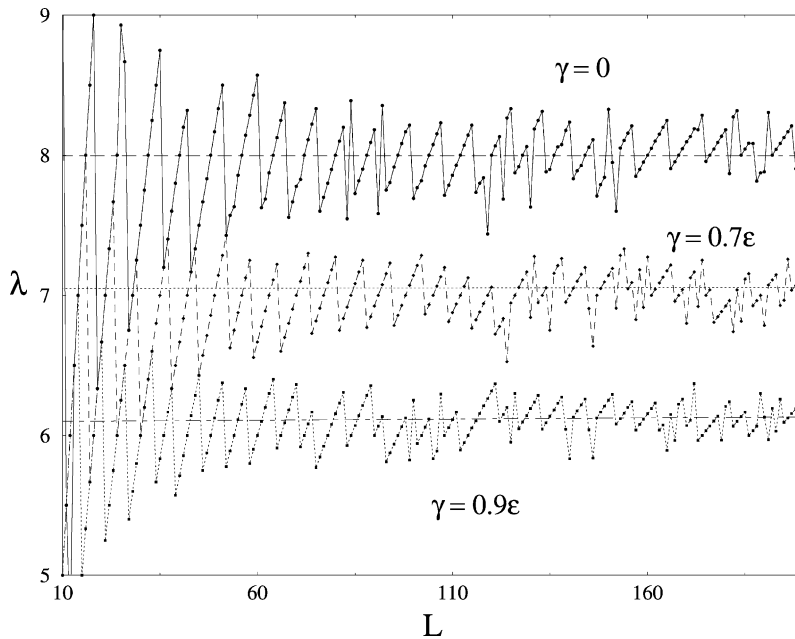


Fig. 9. The wavelength  $\lambda$  as a function of  $L$ . The asymptotic value of  $\lambda$  in the limit  $L \rightarrow \infty$  (horizontal lines) depends on  $\gamma$ .

The sizes of the plateaus increase with  $\lambda$  according to  $\delta \propto \lambda^2$ , as shown in Fig. 6(b).

Fig. 7 shows, with 10 times higher resolution the same plateaus shown in Fig. 6 but on a two-dimensional projection. This figure shows the overwhelming constancy of  $\lambda$  on the plateaus. At the transitions  $\gamma_k$ , it is easy to recognize a regime of ‘hesitation’ between both wavelengths. A careful analysis shows that such hesitation regimes are not spurious but indeed exist.

The wavelength also varies with  $\varepsilon$ . Fig. 8 shows the wavelength as a function of  $\gamma$  and  $\varepsilon$ . The boundaries of successive plateaus of constant wavelength vary quite abruptly and have an overall parabolic shape. In other words, there is a dependency  $|\gamma_k| \propto \varepsilon^{1/2}$  between the characteristic values  $\gamma_k$  and the coupling strength.

So far, all simulations were done for a fixed value of the lattice size  $L$ . In Fig. 9, we show the dependence of the wavelength on  $L$  for three values of  $\gamma$ . For not too big rings ( $L \lesssim 100$ ), one clearly sees a saw-tooth dependence. The discontinuous jumps occur whenever patterns acquire an extra oscillation, with the wavelength abruptly changing from  $L/p$  to  $(L+1)/(p+1)$ ,

$p$  being the number of oscillations in the pattern. From these formulas, one sees why  $\lambda$  grows linearly while  $p$  does not change.

An additional feature of Fig. 9 is the existence of an asymptotic wavelength  $\lambda_\infty \equiv \lim_{L \rightarrow \infty} \lambda_L$ .

## 5. Conclusions

In this paper, we introduced a simple model of coupled map lattices, given by Eq. (2), that in addition to the usual diffusive term  $D_{i,t}$ , contains a new term  $A_{i,t}$  which incorporates the effects of advection through an asymmetry  $\gamma$  in the coupling between neighbors. The contribution due to advection was derived directly from the well-known physical operators, by discretizing them.

An interesting consequence of including advection in lattices of coupled maps is that it provides a natural mechanism to tune the velocity of asymptotic patterns, allowing one to generate velocities that are up to 1000 times greater than the usual ones found in the absence of advection.

An interesting open question concerns the velocity values for both symmetric [8,25] and asymmetric couplings, that are always below one site per step, independently of the propagation direction being positive or negative. A preliminary investigation seems to show this feature to be a consequence of having coupling only between *first* neighbors.

Of great interest for atmospheric applications is the fact that the advection (asymmetry) present in our model was shown to correspond, in a suitable regime, to the geostrophic wind velocity observed in circulating atmospheric systems.

Particularly attractive now is the possibility of using a more realistic model to address rather complex phenomena that have impact in the atmospheric circulation. For instance, the fact that the geostrophic wind depends on the pressure field and that the horizontal trajectories are along the isobars, the horizontal pressure gradient being perpendicular to them [26], indicates that such pressure field may be adequately simulated with two-dimensional lattices of coupled maps. Another promising possibility is to use two-dimensional lattices of coupled maps incorporating advection to simulate ocean convection [27].

While in the present study, two important processes in atmospheric dynamics (more generally, in geophysical fluid dynamics) have been incorporated in the simulation performed with a one-dimensional coupled map lattice, these processes are by no means all inclusive. In fact, convection, a third crucial mechanism in the dynamics of geofluids, has not yet been systematically studied with coupled maps. This is a natural next step which may be implemented by considering two-dimensional lattices of maps coupled not only horizontally but also in the vertical. Among all physical phenomena involving convection, once again, a promising application in geodynamics is the simulation of ocean convection.

## Acknowledgements

This work was supported by the bilateral project 077/2001 sponsored by CAPES (Brazil) and ICCTI

(Portugal), project 133/2001 sponsored by CAPES (Brazil) and DAAD (Germany), by *Fundação para a Ciência e a Tecnologia* and by *Fundação da Faculdade de Ciências da Universidade de Lisboa*, Portugal. JACG is a Senior Research Fellow of the *Conselho Nacional de Desenvolvimento Científico e Tecnológico*, Brazil.

## References

- [1] E.N. Lorenz, *Tellus* 12 (1960) 243–254.
- [2] E.N. Lorenz, *J. Meteorol. Soc. Jpn.* 60 (1982) 255–267.
- [3] G.J. Haltiner, R.T. Williams, *Numerical Prediction and Dynamic Meteorology*, second ed., Wiley, New York, 1980.
- [4] J.R. Holton, *An Introduction to Dynamic Meteorology*, third ed., Academic Press, New York, 1992.
- [5] J.P. Peixoto, A.H. Oort, *Physics of Climate*, American Institute of Physics, New York, 1992.
- [6] A.A. Tsonis, *Int. J. Bif. Chaos* 11 (2001) 881–902.
- [7] K. Kaneko, *Phys. Rev. Lett.* 69 (1992) 905–908; K. Kaneko, *Physica D* 68 (1993) 299–317.
- [8] K. Kaneko, *Complex Systems: Chaos and Beyond*, Springer, Berlin, 2000 and references therein.
- [9] I. Waller, R. Kapral, *Phys. Rev. A* 30 (1984) 2047–2055; R. Kapral, *Phys. Rev. A* 31 (1985) 3868–3879.
- [10] S.P. Kuznetsov, in: K. Kaneko (Ed.), *Theory and Applications of Coupled Map Lattices*, Wiley, Chichester, 1993, pp. 51–94; S.P. Kuznetsov, *Radiophys. Quant. Elect.* 28 (1986) 679–692.
- [11] P.M. Gade, R.E. Amritkar, *Phys. Rev. E* 47 (1993) 143–154.
- [12] V.S. Afraimovich, V.I. Nekorkin, *Int. J. Bif. Chaos* 4 (1994) 631–637.
- [13] V.N. Belykh, E. Mosekilde, *Phys. Rev. E* 54 (1996) 3196–3203.
- [14] R. Coutinho, B. Fernandez, *Physica D* 108 (1997) 60–80.
- [15] P.G. Lind, J. Corte-Real, J.A.C. Gallas, in: S. Boccaletti, J. Burguete, W. Gonzalez-Viñas, H.C. Mancini, D. Valladares (Eds.), *Space Time Chaos: Characterization, Control and Synchronization*, World Scientific, Singapore, 2001, pp. 61–77. <http://www.if.ufrgs.br/~jgallas>.
- [16] K. Kaneko, *Phys. Lett.* 111 (1985) 321–325.
- [17] Y. Jiang, P. Parmananda, *Phys. Rev. E* 57 (1998) R2499–R2502; Y. Jiang, *Phys. Lett. A* 240 (1998) 60–64.
- [18] I.S. Aranson, A.V. Gaponov-Grekhov, M.I. Rabinovich, *Physica D* 33 (1988) 1–20.
- [19] I. Aranson, D. Golomb, H. Sompolinsky, *Phys. Rev. Lett.* 68 (1992) 3495–3498.
- [20] F. Schmöser, W. Just, *J. Stat. Phys.* 105 (2001) 525–559.
- [21] F.H. Willeboordse, K. Kaneko, *Phys. Rev. Lett.* 73 (1994) 533–536; F.H. Willeboordse, K. Kaneko, *Physica D* 86 (1995) 428–455.

- [22] P.G. Lind, J. Corte-Real, J.A.C. Gallas, *Physica A* 295 (2001) 297–300.
- [23] L.D. Landau, E.M. Lifshitz, *Course of Theoretical Physics, Fluid Mechanics*, Vol. VI, Pergamon Press, Oxford, 1959.
- [24] M.W. Beims, J.A.C. Gallas, *Physica A* 238 (1997) 225–244.
- [25] P.G. Lind, J. Corte-Real, J.A.C. Gallas, *Int. J. Bif. Chaos* 11 (2001) 2647–2661.
- [26] J.F. Nye, A.S. Thorndike, *J. Phys. A* 13 (1980) 1–14; A.S. Thorndike, C.R. Cooley, J.F. Nye, *J. Phys. A* 11 (1978) 1455–1490.
- [27] P. Lind, S. Titz, T. Kuhlbrodt, J.A.M. Corte-Real, J. Kurths, J.A.C. Gallas, U. Feudel, Coupled bistable maps: a tool to study convection parameterization in ocean models, *Phys. Rev. E*, submitted for publication.